Supporting Information

Indole and Triazole Containing Ferrocene-Based Two-Terminal Resistive Memory Devices

Abhik Ghoshal[1], Pinki Pal[2], Rajwinder Kaur[1], Semanti Das[1], Pradeep Sachan[1], and Prakash Chandra Mondal[1,*]

[1]Department of Chemistry, Indian Institute of Technology Kanpur, Uttar Pradesh-208 016, India

[2]Department of Chemistry, School of Engineering, Presidency University, Bengaluru, Karnataka 560119, India

E-mail: pinki.pal@presidencyuniversity.in (P.P); pcmondal@iitk.ac.in (P.C.M.)

List of Contents

1. Materials

Ferrocene carboxaldehyde 1 and tryptamine 2 were purchased from Sigma-Aldrich (India). 4-amino-4H-1,2,4-triazole from Avra (99%) (Telangana, India) and used without further purification. All glassware, sourced from Borosil Technology (Mumbai, India), was thoroughly cleaned using chromic acid and an alkaline bath, followed by extensive rinsing with deionized water and subsequently dried in a hot oven at 70 °C for 5 hours. The bottom electrode in the device architecture consisted of a single-side coated indium tin oxide (ITO) glass substrate (Nano Shel UK Ltd.), featuring a thickness of 1.1 mm, a sheet resistance below 10 Ω/sq, and an optical transmittance exceeding 83% in the visible spectrum. Prior to use, the ITO substrates were sequentially cleaned with anhydrous hexane (99%), acetone (≥ 99%), and isopropyl alcohol (≥ 99%), all obtained from Finar Limited, India. After the cleaning process, the substrates were dried and purged with high-purity nitrogen gas for 20 minutes to eliminate residual solvents and moisture before performing electrochemical measurements. Thin films were deposited using anhydrous acetonitrile (99%), acquired from Rankem, India.

2. Synthesis of ferrocene derivatives

2.1. Synthesis of Fc-1

The new ferrocene Schiff base ligand was prepared by mixing ferrocene carboxaldehyde **1** (100 mg, 0.47 mmol) and tryptamine **2** (83 mg, 0.52 mmol) in 10 mL absolute ethanol and reflux for 2 h at 65°C. The reaction was monitored by TLC. After completion of the reaction the crude product was recrystallized by $CHCl_3$/hexane to get light brown solid ferrocene Schiff base **3**. ^{1}H NMR (500 MHz, $CDCl_3$): δ 7.98 (d, *J* = 18.9 Hz, 2H), 7.68 (d, *J* = 7.8 Hz, 1H), 7.34 (d, *J* = 8.0 Hz, 1H), 7.19 (t, *J* = 7.3 Hz, 1H), 7.13 (t, *J* = 7.4 Hz, 1H), 7.05 (s, 1H), 4.58 (s, 2H), 4.32 (s, 2H), 4.03 (s, 5H), 3.79 (t, *J* = 7.1 Hz, 2H), 3.14 (s, 2H).

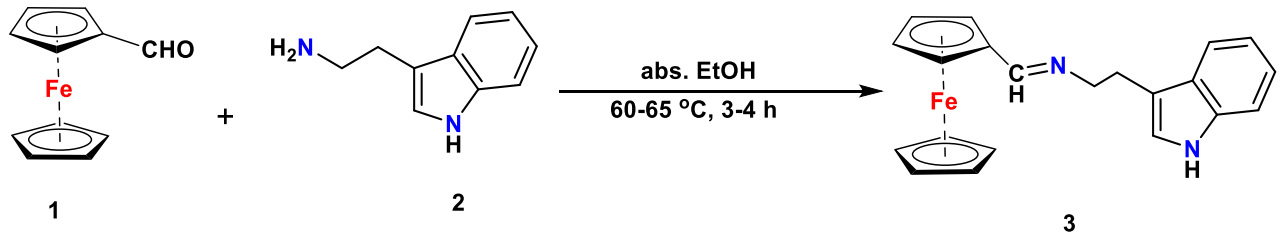

Scheme S1: Synthesis scheme of Fc-1.

2.2 Synthesis of Fc-2

To a solution of ferrocene carboxaldehyde **1** (100 mg, 0.46 mmol) in abs. EtOH (20 mL) was added 4-amino-4H-1,2,4-triazole **2** (43 mg, 0.51 mmol), and the mixture was stirred under reflux for 2 hrs until completion of the reaction (TLC control). The resulting reaction mixture was cooled to room temperature and evaporate the solvent to get solid product. The solid residue was recrystallized with $CHCl_3$/ hexane (1:3) to get the pure compound **3**. ^{1}H NMR (500 MHz, $CDCl_3$): δ 8.49 (s, 2H), 8.46 (s, 1H), 4.69 (s, 2H), 4.58 (s, 2H), 4.26 (s, 5H).

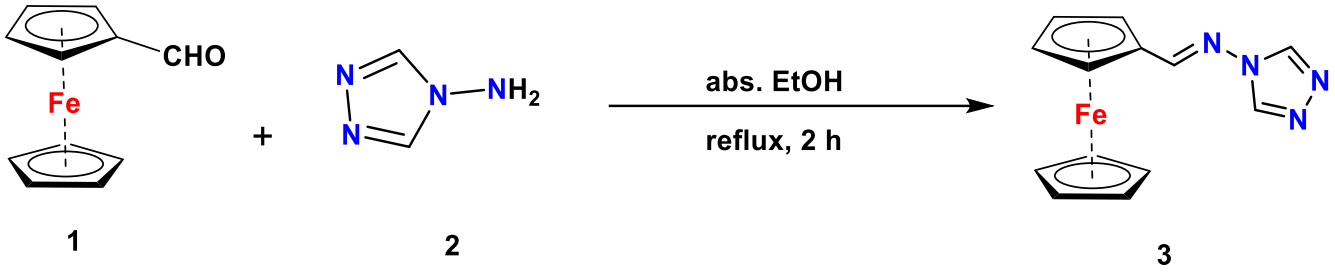

Scheme S2: Synthesis scheme of Fc-2.

3. Characterization Data (^{1}H NMR, and Mass spectrum)

3.1. ^{1}H NMR of Fc-1

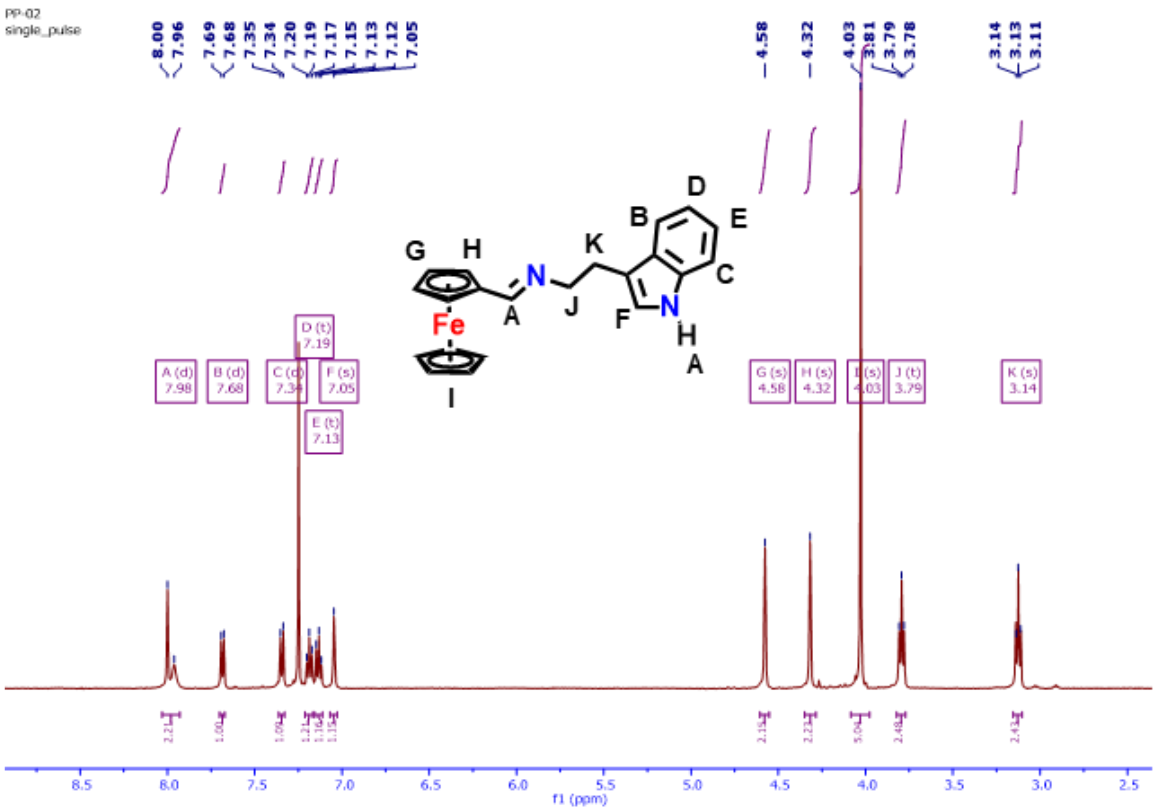

Figure S1. ^{1}H NMR of Fc-1 (500 MHz, recorded in $CDCl_3$).

3.2 ^{1}H NMR of Fc-2

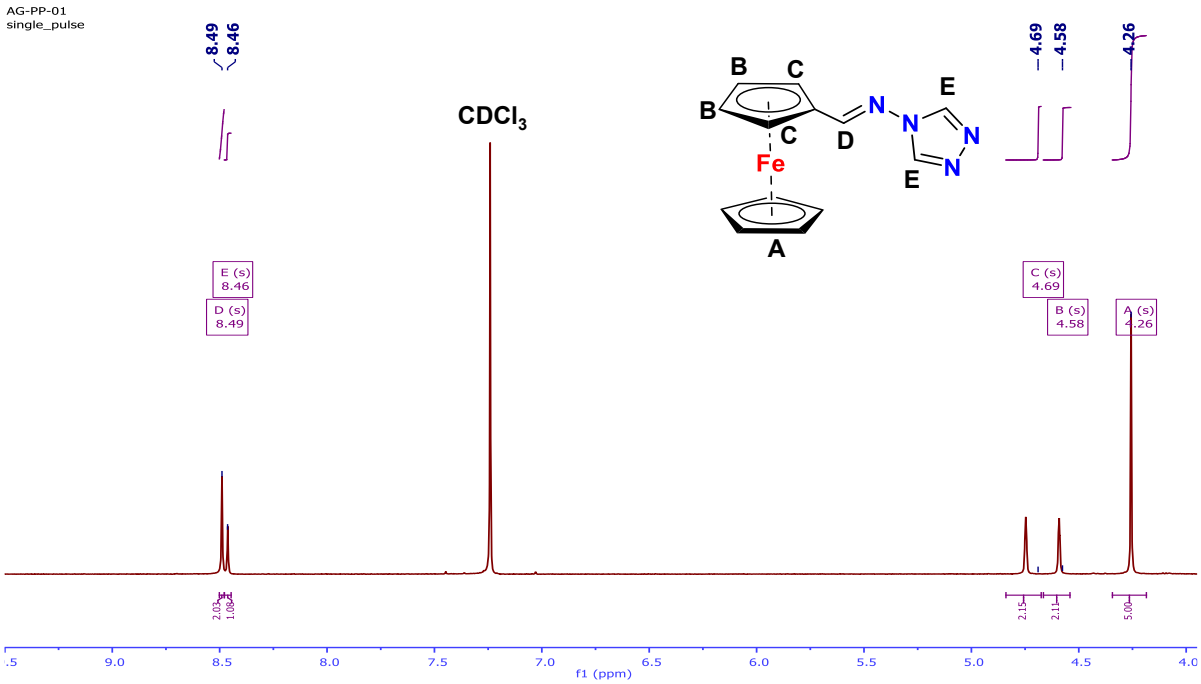

Figure S2. ^{1}H NMR of Fc-2 (500 MHz, recorded in $CDCl_3$).

3.3 High-resolution mass spectrum of Fc-1

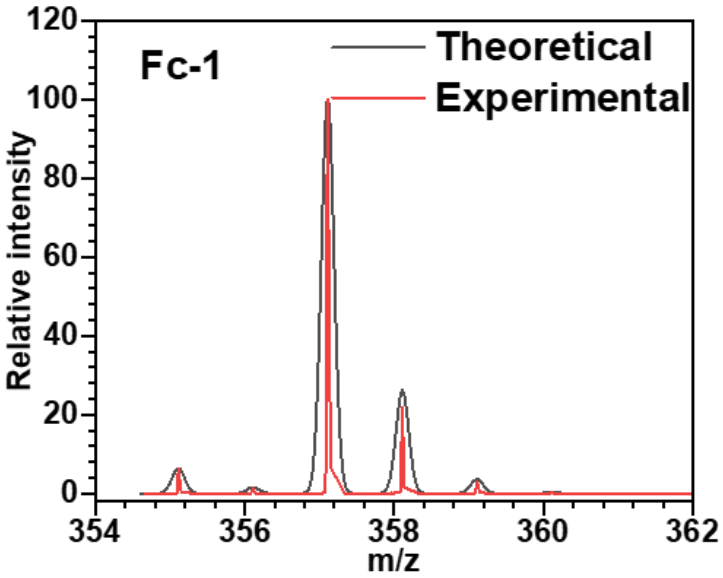

Figure S3. High-resolution mass spectrum (ESI-MS, positive mode) for Fc-1.

3.4 High-resolution mass spectrum of Fc-2

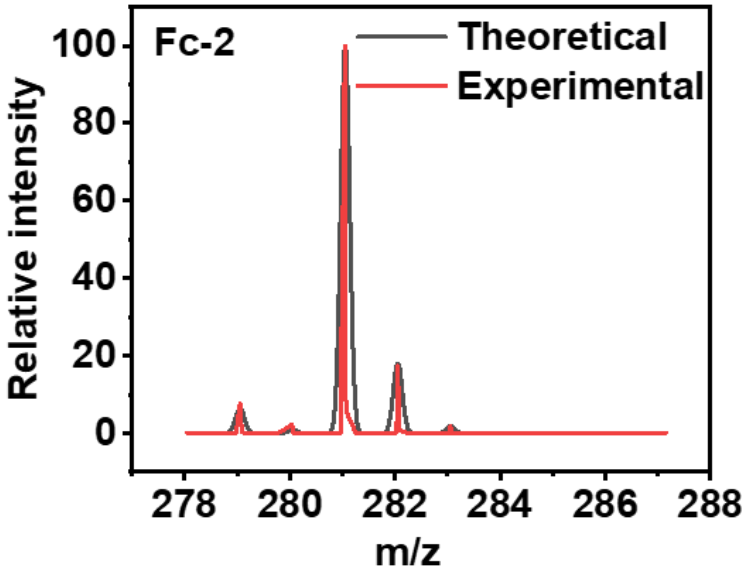

Figure S4. High-resolution mass spectrum (ESI-MS, positive mode) for Fc-2.

4. Solution phase electrochemical measurements of Fc-1, and Fc-2

Table S1: Scan rate-dependent redox parameters of Fc-1, and Fc-2 obtained from cyclic voltammograms in acetonitrile solution. All potential (E) values are presented vs. $Ag/AgNO_3$.

Compounds	Scan rate (mVs^{-1})	$E_{p,a}$ (V)	$E_{p,c}$ (V)	ΔEp (V)	$E_{1/2}$ (V)	$i_{p,a}$ (mA cm^{-2})	$i_{p,c}$ (mA cm^{-2})	$i_{p,a}/i_{p,c}$
Fc-1	10	0.316	0.222	0.094	0.27	0.1429	0.112	0.78
	20	0.320	0.227	0.093	0.273	0.1824	0.147	0.81
	30	0.331	0.230	0.101	0.280	0.221	0.208	0.92
	50	0.344	0.224	0.120	0.284	0.2284	0.203	0.90
	100	0.369	0.204	0.165	0.286	0.2795	0.275	0.99
Fc-2	10	0.244	0.170	0.074	0.207	0.034	0.033	1.03
	20	0.245	0.169	0.076	0.207	0.052	0.051	1.01
	30	0.247	0.167	0.08	0.207	0.067	0.068	0.99
	40	0.248	0.167	0.081	0.208	0.077	0.079	0.99
	50	0.251	0.167	0.084	0.209	0.088	0.090	0.99
	100	0.257	0.161	0.096	0.209	0.121	0.129	0.94

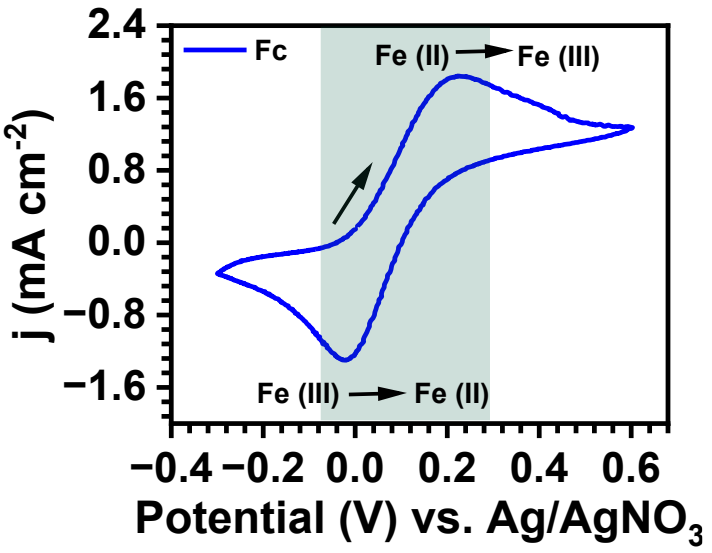

Figure S5: Solution phase electrochemical measurements of Ferrocene in acetonitrile solution with scan rate 100 mV s^{-1}, using ITO, $Ag/AgNO_3$ and pt wire as working, reference and counter electrodes respectively.

5. Diffusion coefficient calculation of Fc-1, and Fc-2 from scan rate dependent CV

To calculate the diffusion coefficient (D in cm^2 s^{-1}), the Randles–Sevcik equation was used, were,

$$i_p = (2.69 \times 10^5)\ A \times D^{1/2}\ n^{3/2}\ v^{1/2}\ C$$

Here i_p is the cathodic or anodic peak current, n is the number of electrons, F the Faraday's constant (C mol^{-1}), A is the electrode surface area (in cm^2), C is the concentration of the oxidative or reductive species (mol cm^{-3}), T the temperature (K) and v is scan rate in V s^{-1}. [1]

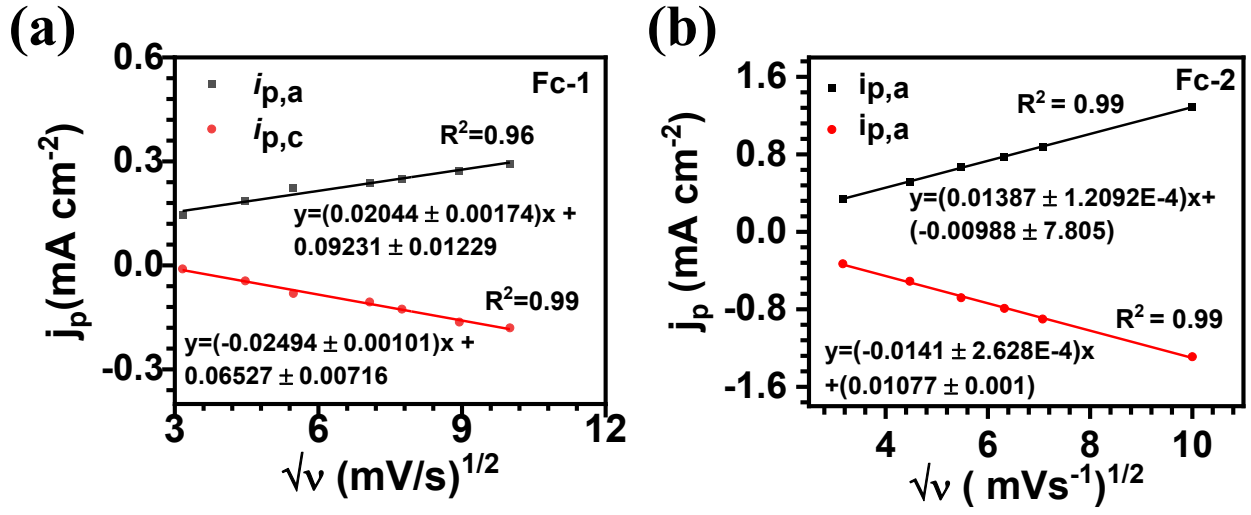

Figure S6: Peak current vs. scan rate plot of (a) Fc-1, and (b) Fc-2.

Table S2: Determination of diffusion coefficients for oxidation and reduction of Fc derivatives

Compound	Slope	D ($cm^2 s^{-1}$)	Average D ($cm^2 s^{-1}$)
Fc-1	0.024 ± 0.002	0.8×10^{-5} (Fc)	1.0×10^{-5}
	0.025 ± 0.001	1.2×10^{-5}(Fc^+)	
Fc-2	0.014 ± $1.209*10^{-4}$	0.26×10^{-5}(Fc)	0.265×10^{-5}
	0.014 ± 2.628^{-4}	0.27×10^{-5}(Fc^+)	

6. Density functional theory study

Fc-1, and Fc-2 structures were optimized using B3LYP level 6-311g (d,p) basis set for the (C, H, N, Fe), further studied with the help of GaussView6.0.16.

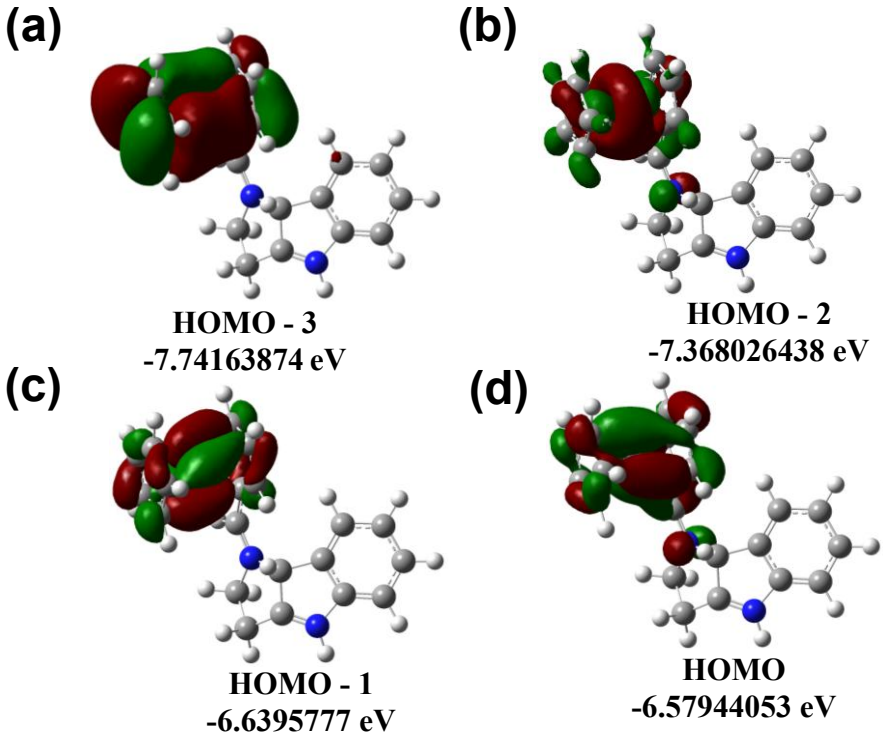

Figure S7: Orbital energy diagram of HOMO for Fc-1.

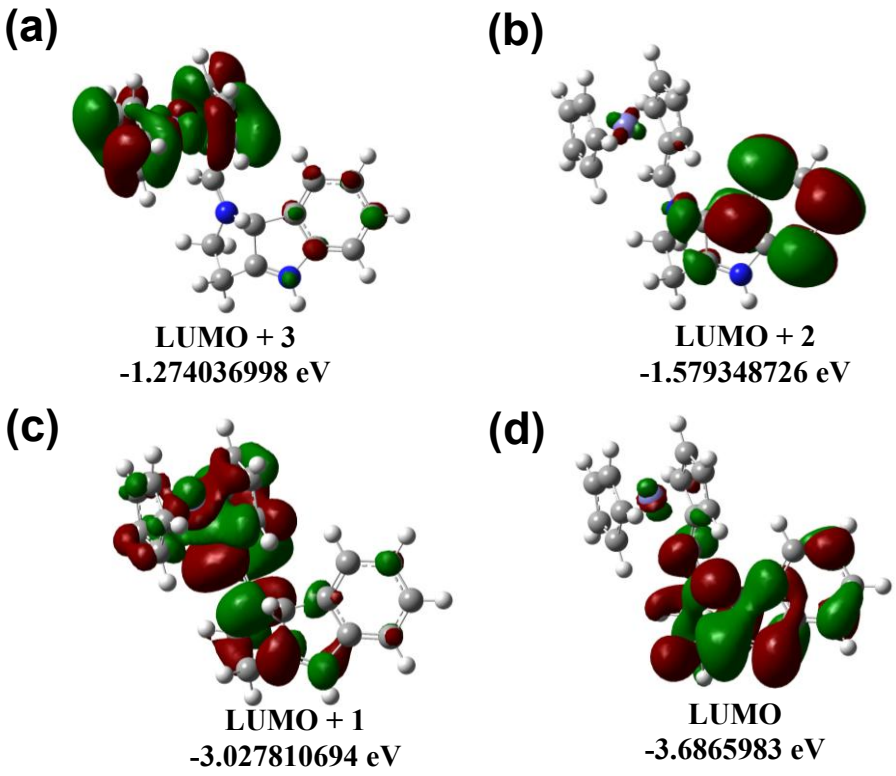

Figure S8: Orbital energy diagram of LUMO for Fc-1.

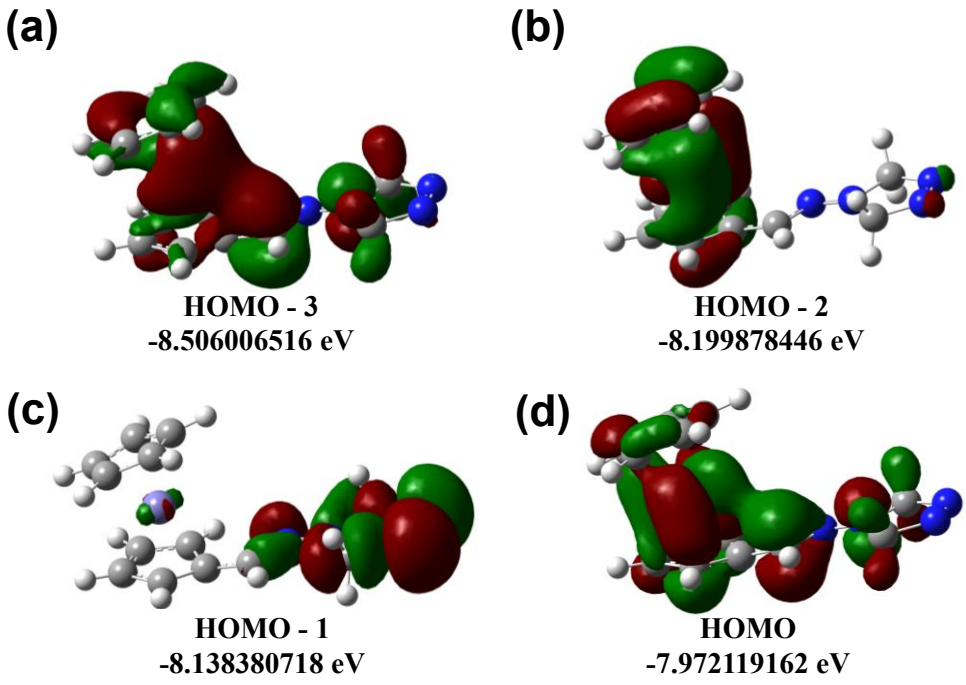

Figure S9: Orbital energy diagram of HOMO for Fc-2.

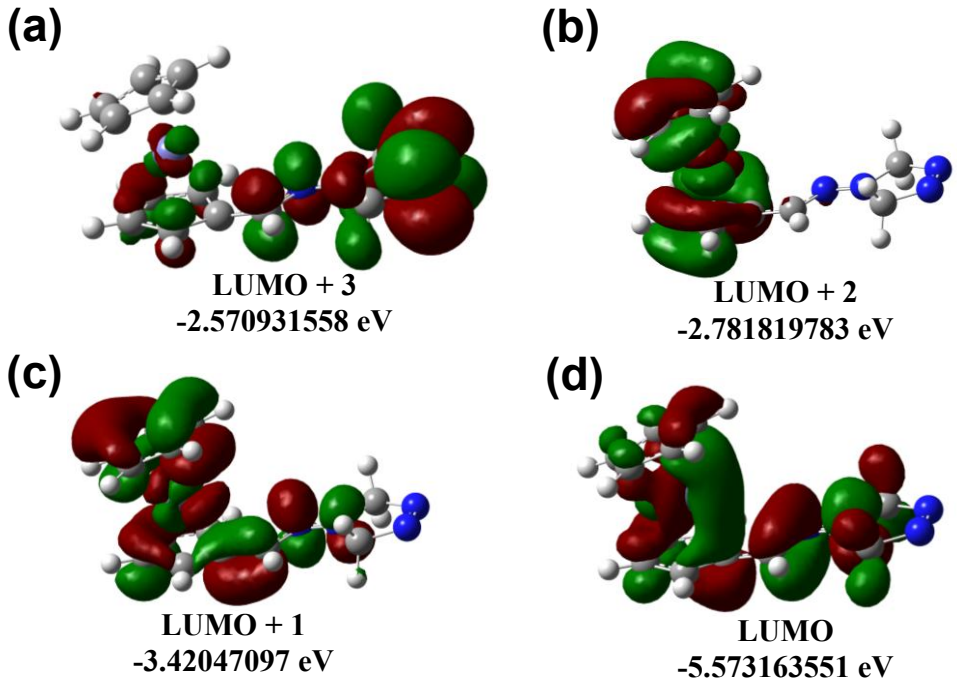

Figure S10: Orbital energy diagram of LUMO for Fc-2.

Table S3: Energies of the frontier orbitals (HOMO-3 to LUMO+3) of **Fc1** and **Fc2** complexes.

S. No.	Orbital	Energy in eV	
		Fc 1	Fc 2
1.	LUMO + 3	-1.274036998	-2.570931558
2.	LUMO + 2	-1.579348726	-2.781819783
3.	LUMO + 1	-3.027810694	-3.42047097
4.	LUMO	-3.6865983	-5.573163551
5.	HOMO	-6.57944053	-7.972119162
6.	HOMO -1	-6.6395777	-8.138380718
7.	HOMO - 2	-7.368026438	-8.199878446
8.	HOMO - 3	-7.74163874	-8.506006516
9.	Band gap	2.89284223	2.398955611

7. Thin film optical characterization of Fc-1, and Fc-2

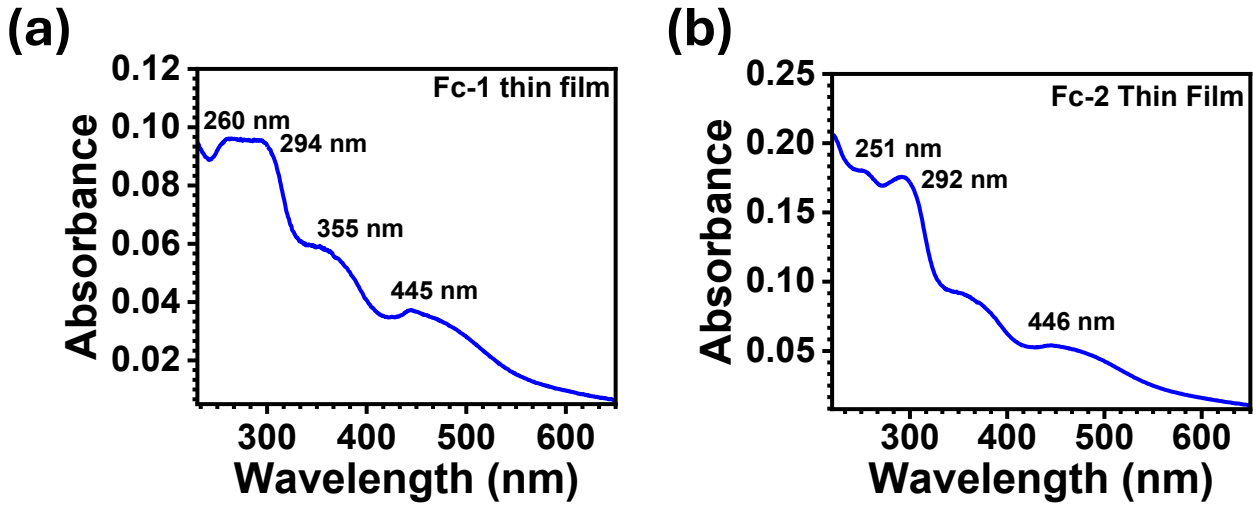

Figure S11: UV-vis characterization of (a) Fc-1, and (b) Fc-2 thin film deposited on quartz substrate.

Thin film UV-vis measurements were performed by depositing thin films of Fc-1, and Fc-2 on quartz substrate. For Fc-1, characteristic absorption peaks at 260 nm, 294 nm, 355 nm, and 445 nm corresponds to π→π* of indole moiety, π→π* of ferrocene, to n→π* of the ligand framework, and d-d transitions of Fe respectively. Similarly, For Fc-2, characteristic absorption peaks at 251 nm, 292 nm corresponds to π→π* of triazole ring and cyclopentadienyl moiety. Whereas, peaks at 354 nm, and 446 nm are corresponding to n→π*, and d-d transitions of Fe respectively.

8. Calculation of optical bandgap of Fc-1, and Fc-2 from Tauc plot

The optical band gaps of the ferrocene molecules (Fc-1 and Fc-2) were determined using Tauc plots. This analysis is based on the Davis and Mott equation, which describes the relationship between a material's optical absorption and the photon energy, providing insight into its band gap. The equation is expressed as follows:

$$(\boldsymbol{\alpha h\nu})^{\mathbf{1/n}} = \left(\boldsymbol{h\nu - E_g}\right) \qquad \textbf{.....S(i)}$$

Here, α is the absorption coefficient, h Planck constant (4.135×10^{-15} eV.s), ν is the photon's frequency (s^{-1}) and E_g is the band gap.

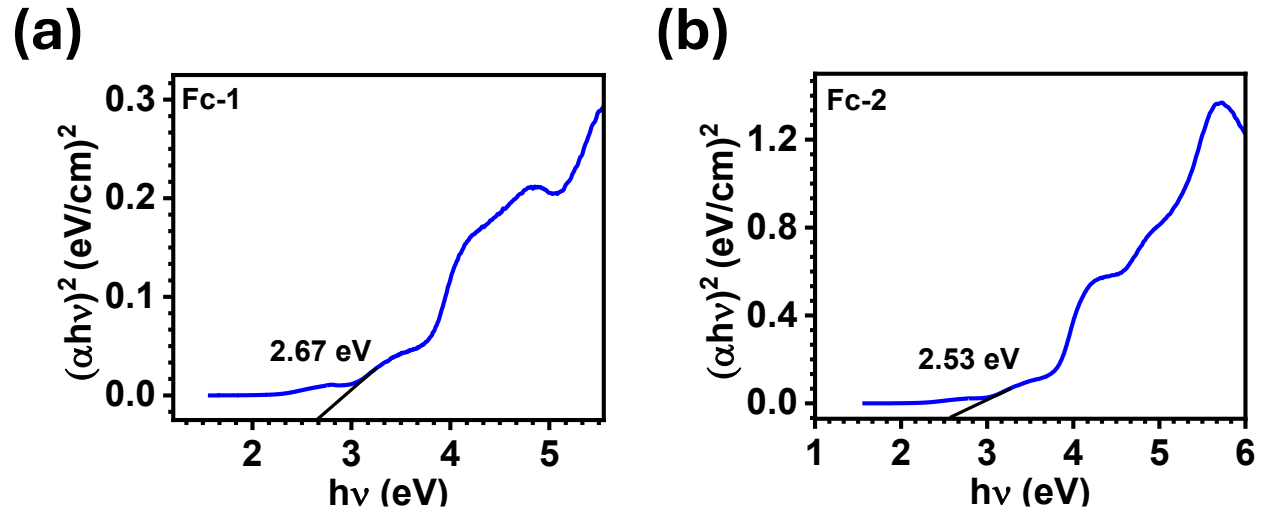

Figure S12: Determination of optical bandgap of Fc derivatives. Tauc plot of (a) Fc-1, and (b) Fc-2.

9. Thin film cyclic voltammogram of Fc-1 and Fc-2

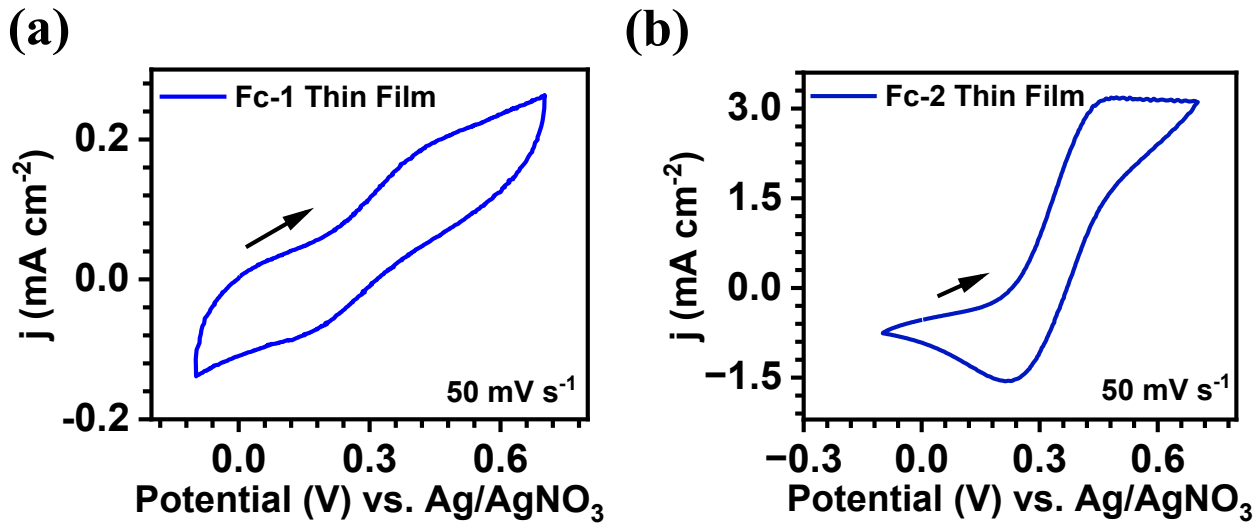

Figure S13: Thin film electrochemical measurements of Ferrocene derivatives. Cyclic voltammogram of (a) Fc-1, and (b) Fc-2 thin film deposited on ITO. $Ag/AgNO_3$ and Pt wire were used as reference, and counter electrodes respectively.

10. Calculation of HOMO and LUMO energy levels in Fc-1, and Fc-2

Understanding the Highest Occupied Molecular Orbital (HOMO) and the Lowest Unoccupied Molecular Orbital (LUMO) is fundamental in molecular electronics, as they control charge transport, influence electronic transitions, and can impact device performance significantly.

The HOMO and LUMO of the ferrocene derivatives were calculated using thin film the UV-Vis and CV data. The HOMO of Fc-2 was calculated using the following formula equation S(ii)

$$E_{HOMO} = - [E_{ONSET} - E_{1/2\ Fc/Fc^+} + 4.8] \qquad \text{.....S(ii)}$$

E_{ONSET} is the onset oxidation potential calculated from the thin film CV, and $E_{1/_{2}Fc/F^{c+}}$ is the Ferrocenium half wave potential (0.121 eV). The LUMO energy value can then be calculated as equation S(iii)

$$E_{LUMO} = E_{HOMO} + E_g \quad \text{……(S (iii)}$$

Where E_g is the band gap energy as calculated from thin film UV.

For Fc-2, E_{ONSET} is calculated as 0.232 V. Hence,

$$E_{HOM0} = -[\,0.232 - 0.121 + 4 \cdot 8] = -4.90 \text{ eV} \quad \text{…….(S (iv)}$$

Taking band gap energy, 2.42 eV as calculated from the Tauc plot,

$$E_{LUM0} = -2.48 \text{ eV}$$

Similarly, for Fc-1, the calculated HOMO, and LUMO energy values are – 4.97 eV, and – 2.11 eV respectively**.**

11. XPS analysis of Fc-1, and Fc-2 thin film on ITO

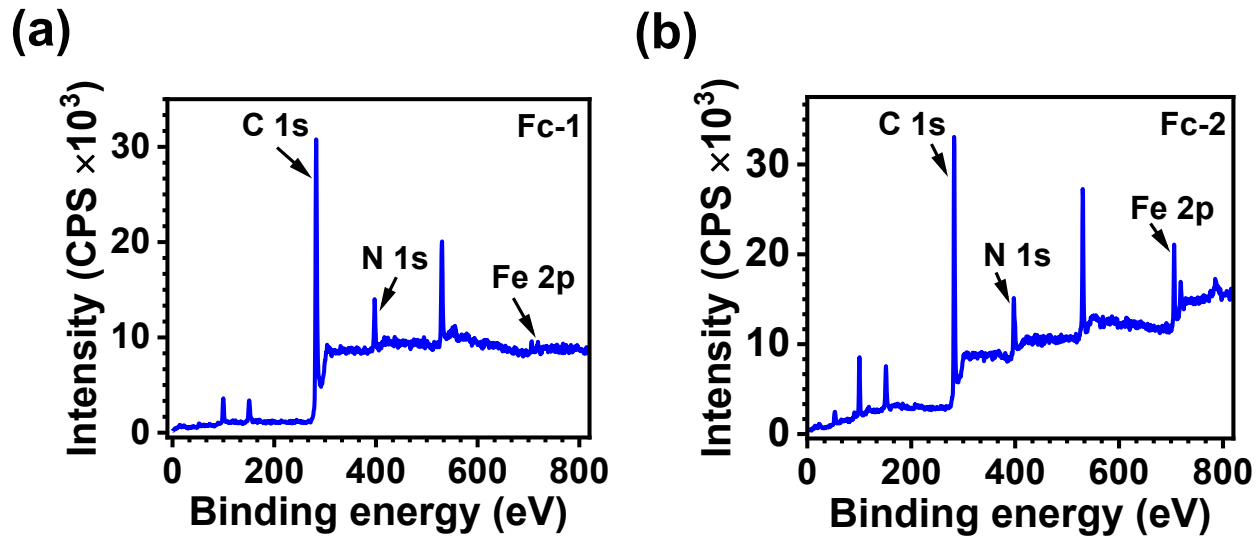

Figure S14: XPS survey scan of (a) Fc-1, and (b) Fc-2 thin film, showing all the characteristic signals.

Table S4: XPS analysis of ITO/Fc thin films

S.N.	Material	Element	State/Term	Binding energy (eV)
1.	ITO/Fc-1	C	1s (C-C/C=C) 1s (C-N, indole) 1s (C=N, imine)	284.6 ± 0.02 285.3 ± 0.06 286.6 ± 0.08
		N	1s (indole) 1s (imine)	398.8 ± 0.20 400.1 ± 0.10
		Fe	$2p_{3/2}$ $2p_{1/2}$	707.6 ± 0.02 720.8 ± 0.05
2.	ITO/Fc-2	C	1s (C-C/C=C) 1s (C=N, imine) 1s (triazole)	284.8 ± 0. 02 286.1 ± 0.04 286.3 ± 0.15
		N	1s (pyridinic N) 1s (C=N, imine) 1s (Graphitic N)	399.5 ± 0.20 401.2 ± 0.10 401.5 ± 1.2
			$2p_{3/2}$ $2p_{1/2}$	707.9 ± 0.04 720.8 ± 0.02

12. Surface morphology analysis of ITO/Fc thin film

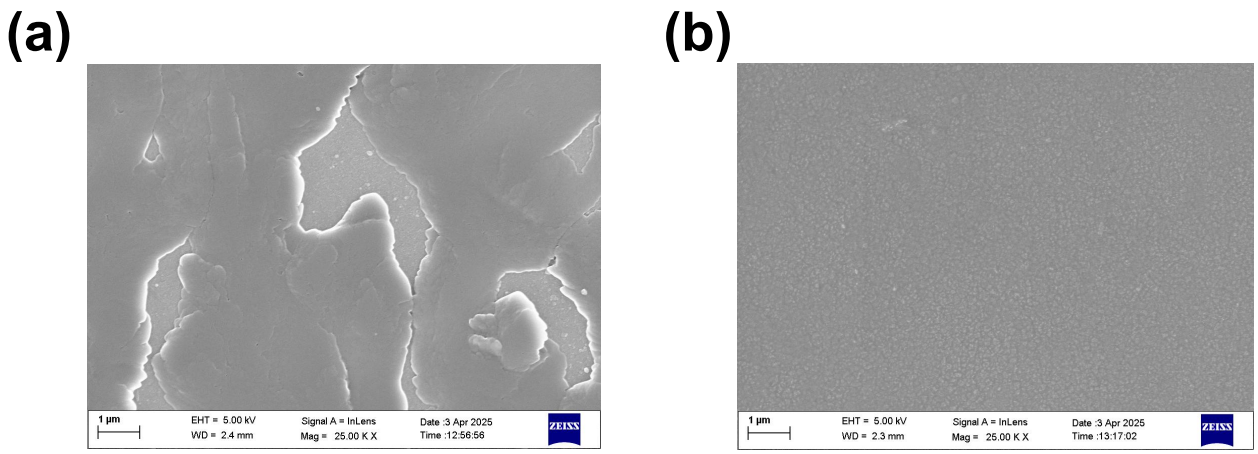

Figure S15: Surface morphological analysis of ITO/Fc thin film**.** FE-SEM image of (a) Fc-1, and (b) Fc-2 thin film on ITO substrate.

13. AFM measurements for calculation of molecular film thickness

The thickness of the Fc-1, and Fc-2 molecular thin film, deposited on ITO was determined using the AFM height profile by scratching a small portion of the film. The difference of average height of the scratched and unscratched portions of the film gives the thickness. Measurements were taken at five different positions and average thickness was calculated.

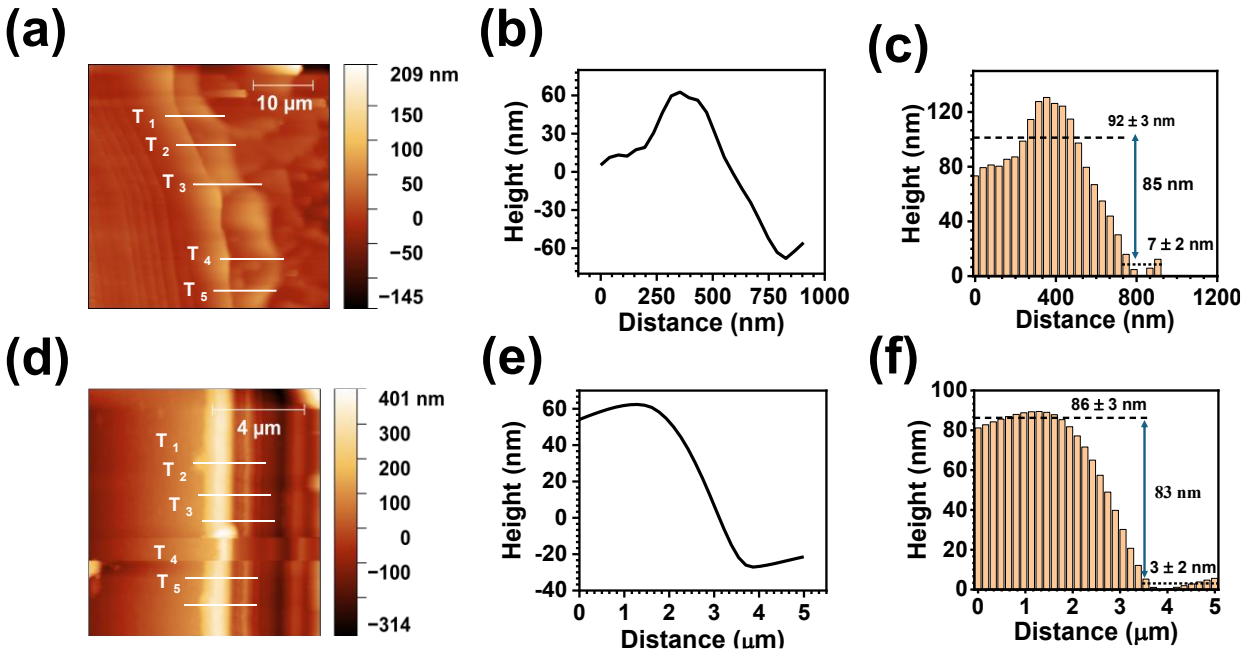

Figure S16: Thickness measurement of ITO/Fc thin films via AFM**.** (a) The AFM topography image of ITO/Fc-1 thin film deposited using a 20 µL solution with 2 mg/mL concentration, revealing uniform film coverage. Line profiles are drawn at five different places for the thickness measurement, (b) a line profile of the thin film, and (c) the corresponding height histogram revealing a film thickness of 85 nm, (d) the AFM topography image of ITO/Fc-2 thin film deposited using a 20 µL solution with 2 mg/mL concentration, and (e) a line profile of the thin film, and (f) the corresponding height histogram showing thickness of 83 nm.

14. AFM measurements for calculation of three additional ITO/Fc-2 film thickness

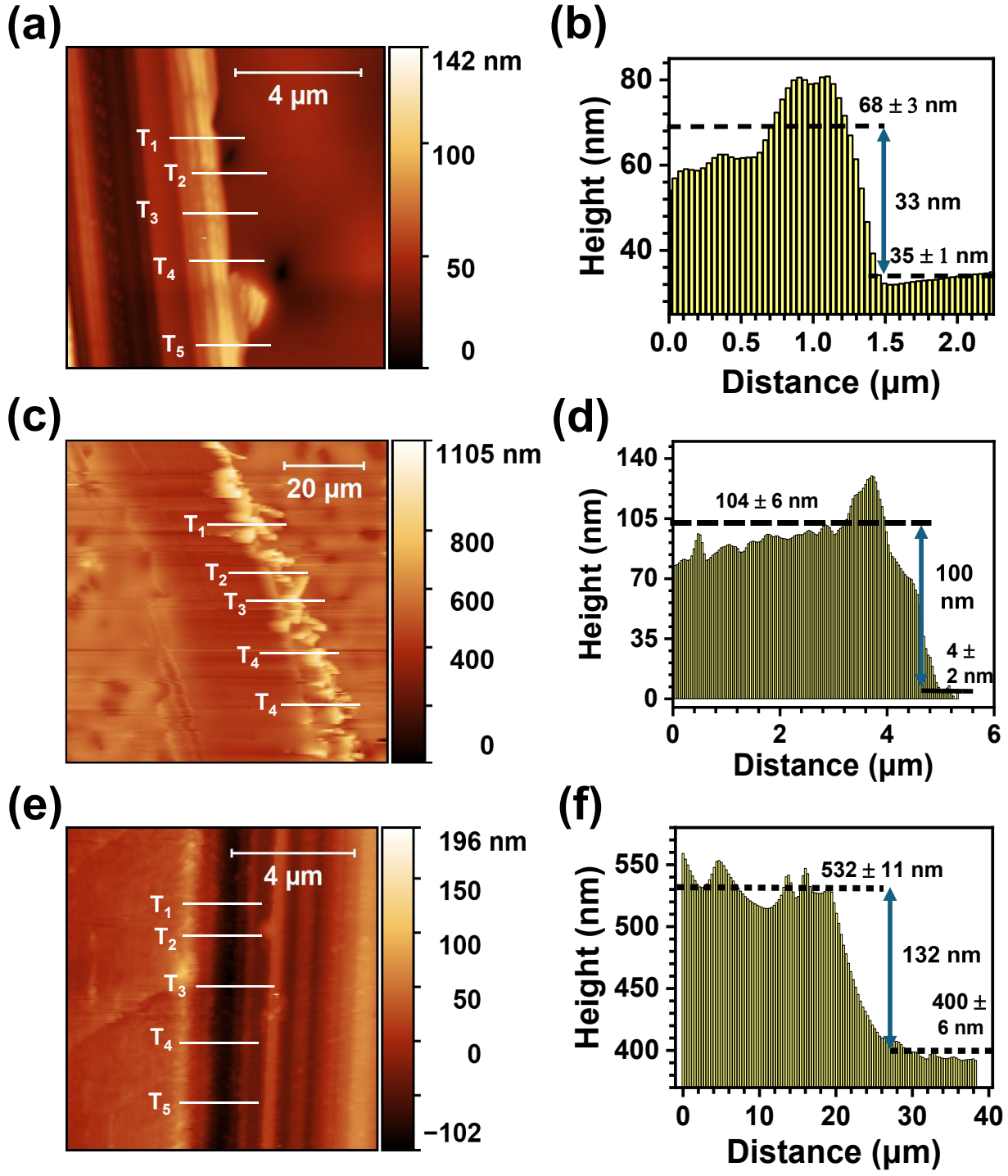

Figure S17: Thickness measurement of three additional ITO/Fc-2 thin films via AFM. (a) the AFM topography image of film 1 deposited using a 20 µL solution with 1 mg/mL concentration, revealing uniform film coverage. Line profiles are drawn at five different places for the thickness measurement. (b) AFM height histogram revealing thin film thickness 33 nm, (c) the AFM topography image of film 2 deposited using a 40 μL solution with 2 mg/mL concentration, revealing uniform film coverage , and (d) AFM height histogram revealing thin film thickness 100 nm, (e) the AFM topography image of film 1 deposited using a 60 μL solution with 1 mg/mL concentration, revealing uniform film coverage, and (f) AFM height histogram revealing thin film thickness 132 nm.

Table S5: Determination of thicknesses of ITO/Fc-1, and ITO/Fc-2 thin films

Film type	Film no.	Line profile	Thickness (nm)	Avg. Thickness (nm)
ITO/Fc-1	1	1	75	80 ± 4
		2	79	
		3	81	
		4	79	
		5	85	
ITO/Fc-2	1	1	41	35 ± 4
		2	30	
		3	35	
		4	33	
		5	34	
	2	1	80	82 ± 3
		2	82	
		3	83	
		4	78	
		5	84	
	3	1	106	105 ± 5
		2	100	
		3	102	
		4	110	
		5	108	
	4	1	150	144 ± 8
		2	140	
		3	132	
		4	144	
		5	154	

15. Memory device fabrication

A solution of ferrocene (Fc-1. Fc-2) derivatives in acetonitrile (20 μL, 2 mg/mL) spin-coated on ITO substrate to form a uniform thin layer. After deposition, the sample was heated at 60 °C for 20 minutes in an oven to remove any residual solvent. An Al electrode, approximately 80 nm thick, was then deposited on the top by thermal evaporation, using a shadow mask to define the electrode pattern. The resistive switching behaviour of the device was evaluated using a two-probe electrical measurement setup.

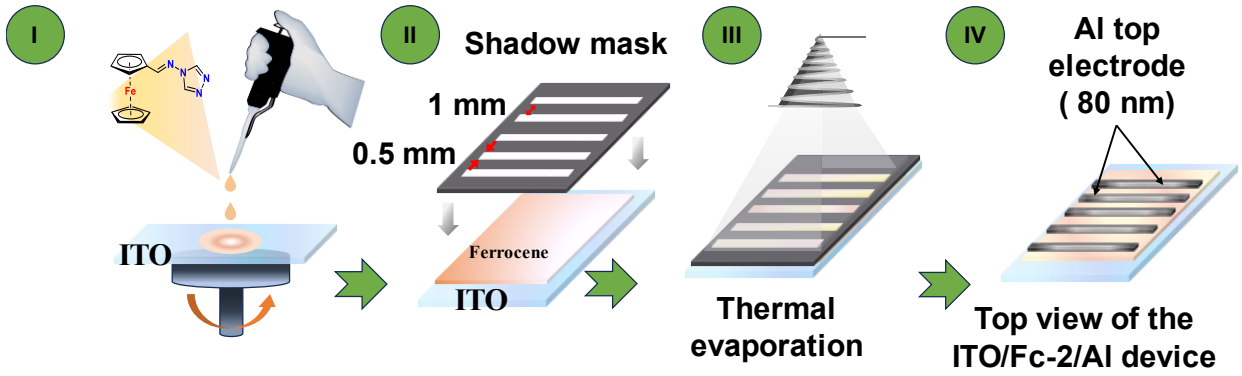

Figure S18: Schematic for fabrication of two-terminal memory device with configuration ITO/Fc-2/Al. The dimension of ITO was 1.5 cm x 0.9 cm.

16. Switching energy Calculation for ITO/Fc/Al

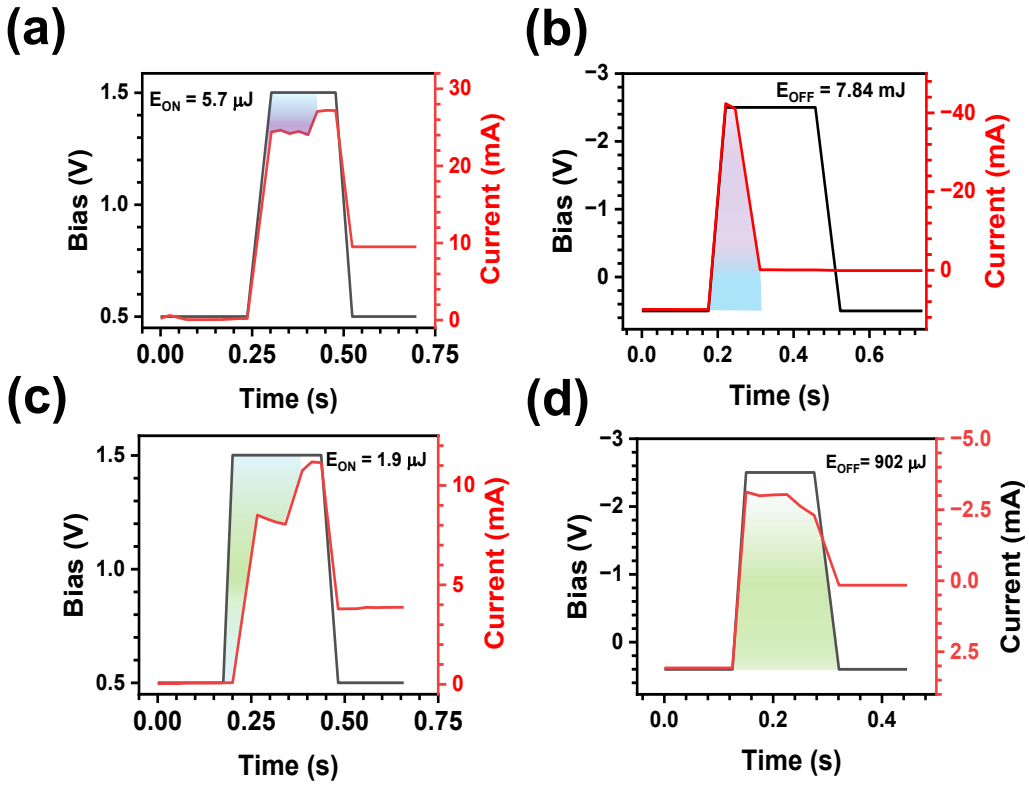

Figure S19: Switching energy calculation for device ITO/Fc-1/Al, (a) SET process, (b) RESET process, and device ITO/Fc-2/Al (c) SET process, (d) RESET process.

To calculate the switching energy of ITO/Fc-1/Al, write pulses with constant amplitude (+ 1.5 V) for 0.18 s are applied with a read voltage of + 0.4 V. The device was initially in an OFF state (**Figure S9a**). Upon application of the + 1.5 V pulse, it turned ON and remained so even after the pulse ended. The corresponding energy (E_{SET}) was calculated as equation S v,[2]

$$E_{SET} = + 1.5 \times \int dI\, dt = 5.7\ \mu J \qquad \text{(S v)}$$

The integral value was calculated from the area of the curve.

By dividing the E_{SET} by switching time to 0.18 s, the power consumption for SET process, P_{SET} = 31.6 μW.

Similarly, for RESET process, the corresponding energy (E_{RESET}) is calculated as equation S vi,

$$E_{RESET} = - 2.5 \times \int dI\, dt = 7.84 \text{ mJ} \qquad \text{(S vi)}$$

By dividing the E_{RESET} by switching time to 0.18 s, P_{SET} = 43.3 mW.

For device ITO/Fc-2/Al. The switching energy corresponding to the SET, and RESET processes are 1.9 μJ, and 902 μJ respectively.

17. I-V characteristics for ITO/Fc-1/Al in different junctions of single device

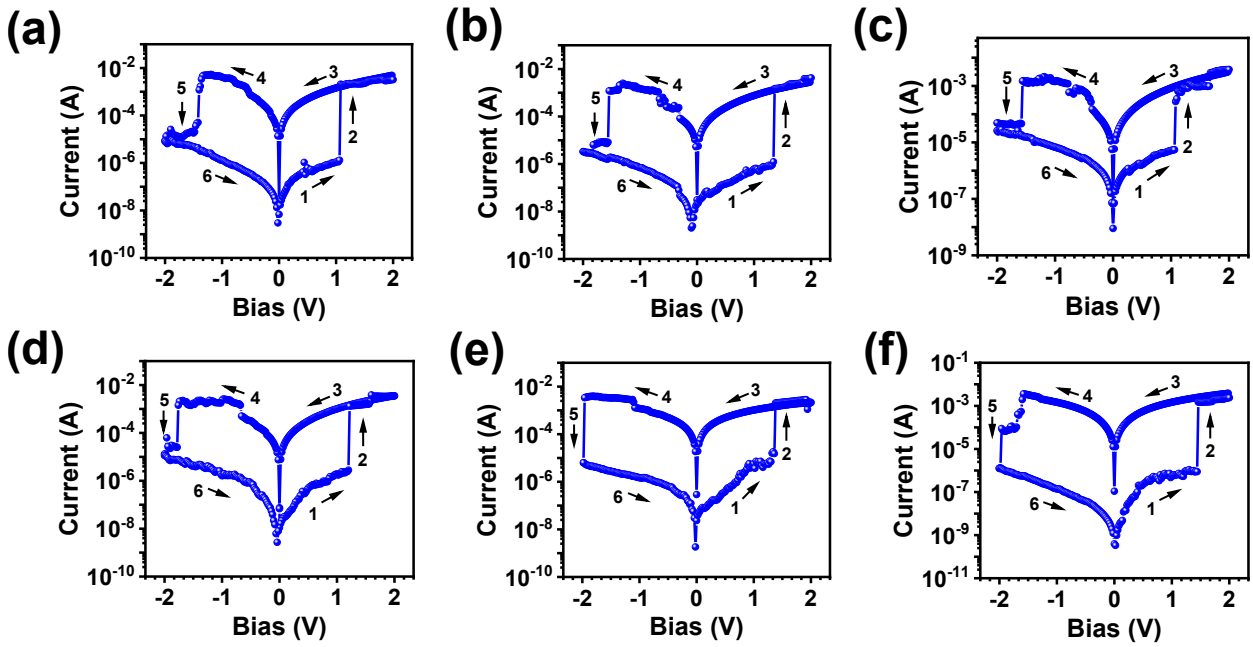

Figure S20: Memory behavior recorded at different junctions in a single device of ITO/Fc-1/Al.

Table S6: **Resistive-switching parameters of device ITO/Fc-1/Al recorded at different junctions**

Junction no.	SET (V)	RESET (V)	$I_{ON/OFF}$
1	+ 1.12	-1.40	3×10^3
2	+ 1.34	-1.55	10^3
3	+ 1.10	-1.56	6×10^2
4	+ 1.22	-1.70	10^3
5	+ 1.35	-1.90	6×10^2
6	+ 1.42	-1.62	10^3

18. Cell-to-cell variation of I-V characteristics for ITO/Fc-1/Al

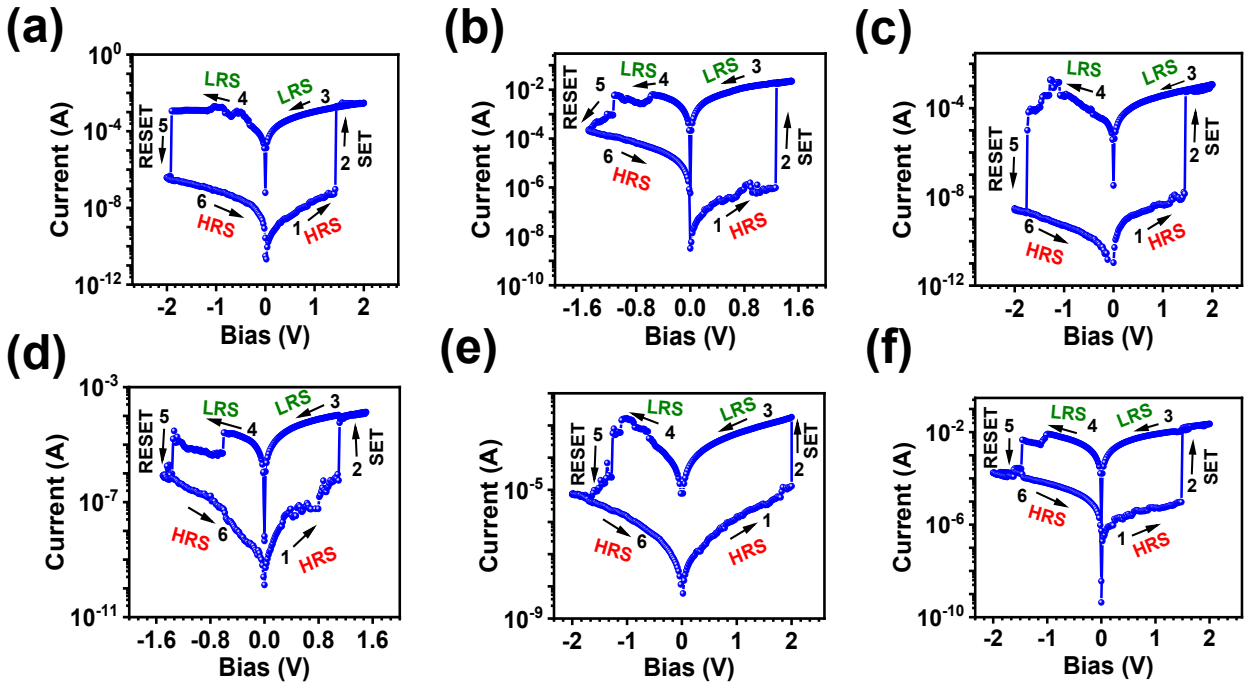

Figure S21: Cell-to-cell reproducibility of the memory behavior in the device ITO/Fc-1/Al.

19. I-V characteristics for ITO/Fc-2/Al in different junctions of single device

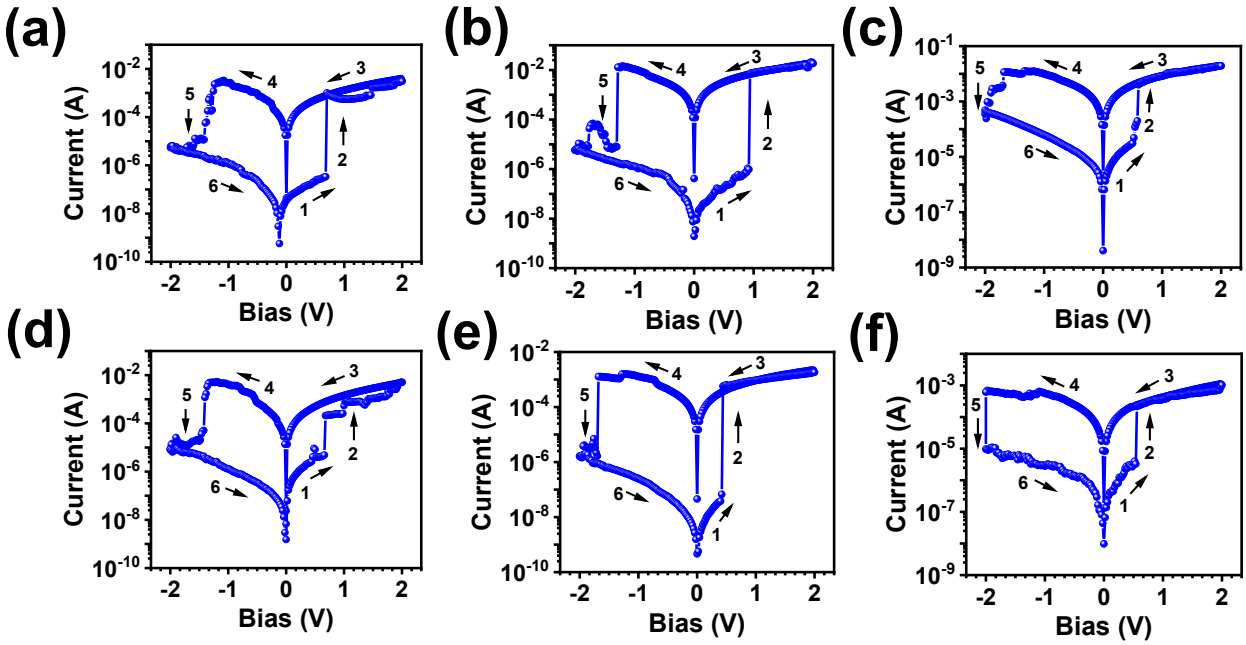

Figure S22: Memory behavior recorded at different junctions in a single device of ITO/Fc-2/Al

Table S7: **Resistive-switching parameters of device ITO/Fc-1/Al recorded at different junctions**

Junction no.	SET (V)	RESET (V)	$I_{ON/OFF}$
1	+ 0.65	- 1.27	10^4
2	+ 0.75	- 1.30	10^4
3	+ 0.52	- 1.68	6×10^2
4	+ 0.65	- 1.35	10^3
5	+ 0.48	- 1.67	10^4
6	+ 0.55	- 1.97	10^2

20. Cell-to-cell variation of I-V characteristics for ITO/Fc-2/Al

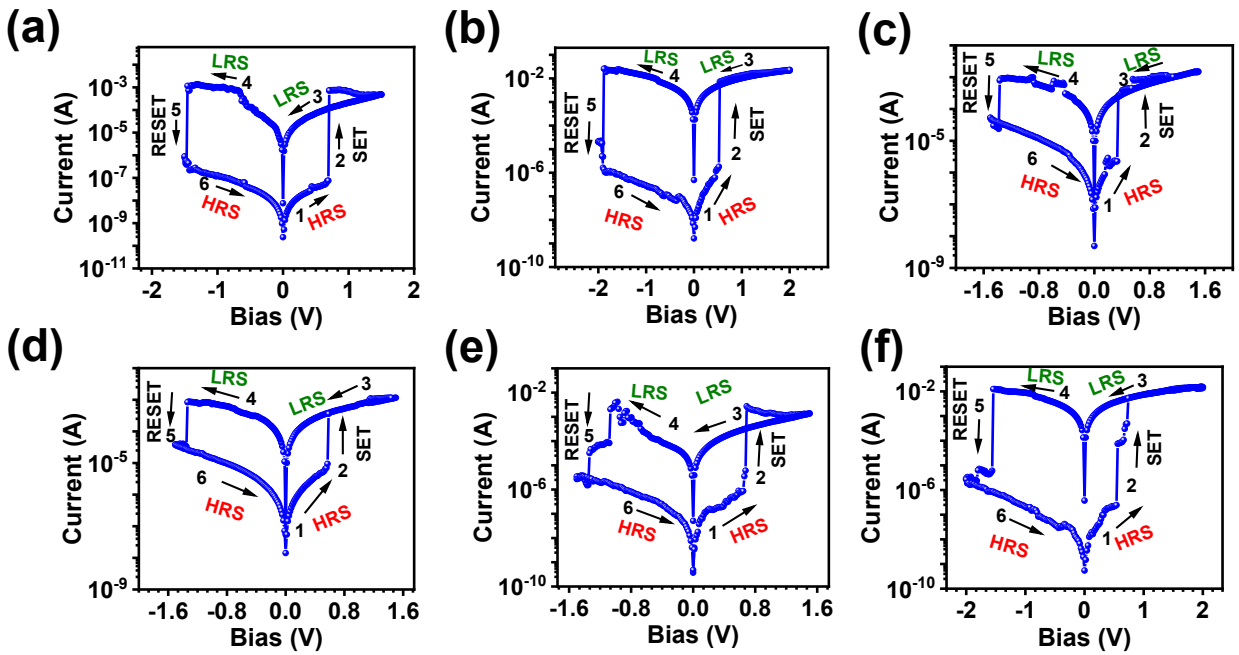

Figure S23: Cell-to-cell reproducibility of the memory behavior in device ITO/Fc-2/Al.

21. Resistive-switching devices: performance and yield

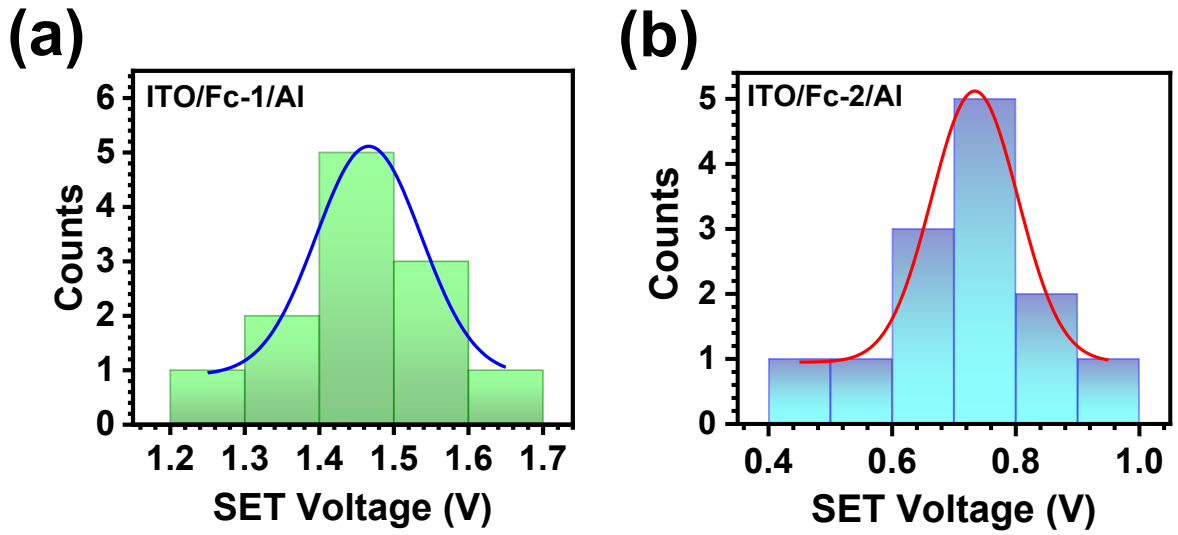

Figure S24: Statistical distribution of the switching voltage (V_{SET}) of the fabricated device (a) ITO/Fc-1/Al, and (b) ITO/Fc-2/Al. The distribution pattern was fitted with gaussian curve.

Table S8. Statistical data of resistive-switching devices of different configuration

Device configuration	Device No.	SET (V)	RESET (V)	$I_{ON/OFF}$
ITO/Fc-1/Al	1	+ 1.42	- 1.90	10^4
	2	+ 1.22	- 1.76	10^3
	3	+ 1.33	- 1.78	2×10^3
	4	+ 1.34	- 1.62	2×10^3
	5	+ 1.33	- 1.60	10^3
	6	+ 1.40	- 1.63	3×10^3
	7	+ 1.34	- 1.58	10^3
	8	+ 1.36	- 1.51	10^3
	9	+ 1.23	- 1.42	3×10^3
	10	+ 1.40	- 1.68	10^4
ITO/Fc-2/Al	1	+ 0.80	- 1.12	2×10^3
	2	+ 0.51	- 1.61	2×10^4
	3	+ 0.52	- 1.80	10^4
	4	+ 0.78	- 1.02	2×10^4
	5	+ 0.53	- 1.80	10^4
	6	+ 0.80	- 1.52	10^4
	7	+ 0.75	- 1.42	10^3
	8	+ 0.62	- 1.44	10^4
	9	+ 0.80	- 1.14	10^4
	10	+ 0.72	- 1.26	5×10^3

22. Determination of switching time for ITO/Fc/Al

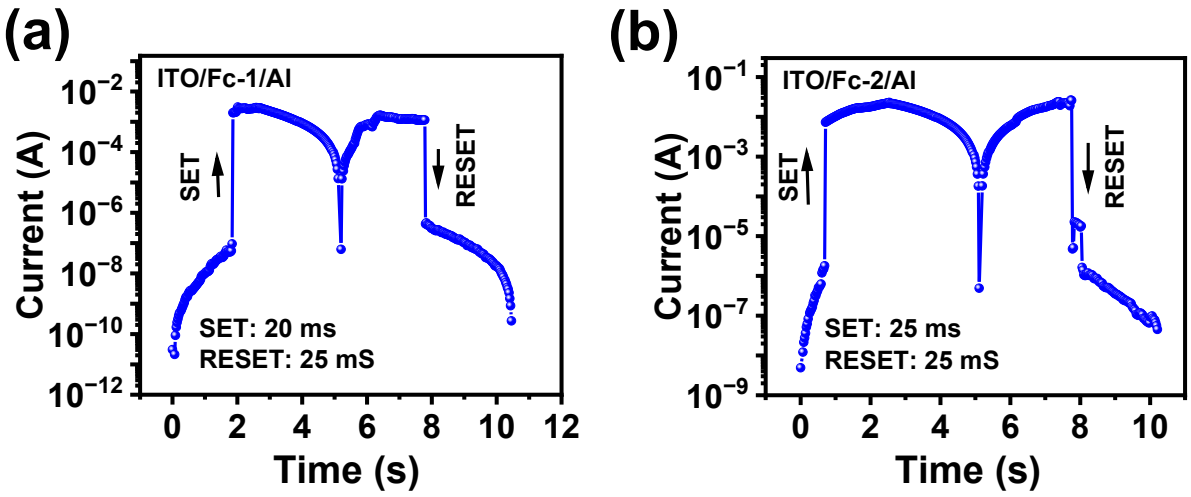

Figure S25: Switching time plots for SET, and RESET processes for device (a) ITO/Fc-1/Al, and (b) ITO/Fc-2/Al.

23. Analysis of non-linear conduction of ITO/Fc-1/Al

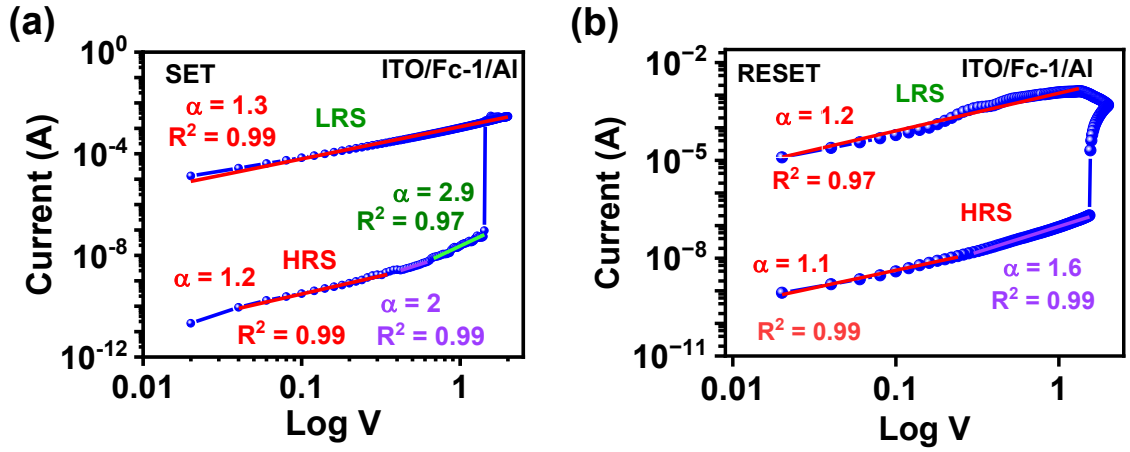

Figure S26: Log-log plot of the device configuration ITO/FC-1/Al, showing Ohmic, and SCLC conduction.

24. I-V characteristics of devices ITO/Fc-1/Au, and ITO/Fc-2/Au

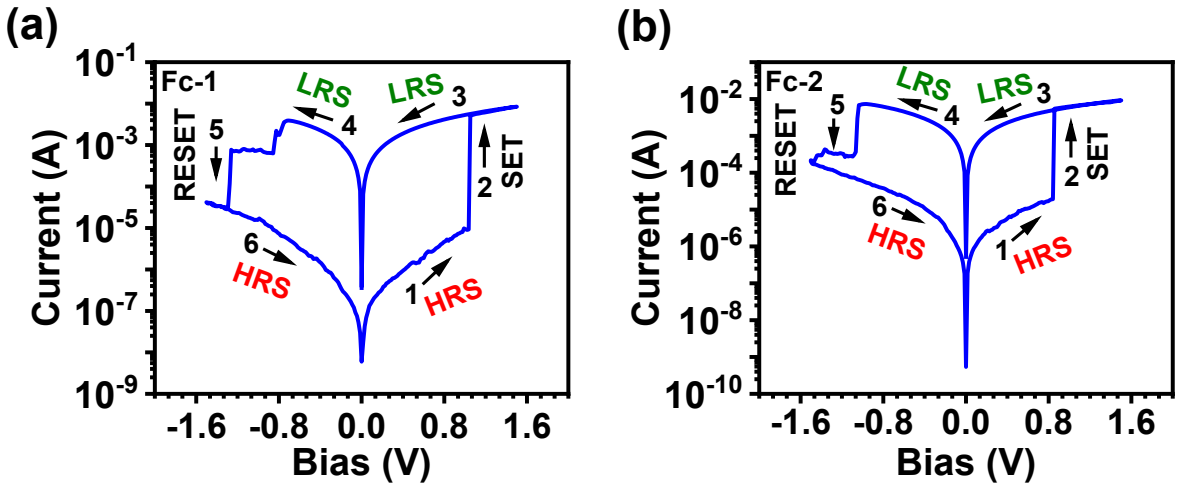

Figure S27: Characteristic memory behavior of Fc derivatives using ITO, and Au as bottom, and top electrodes respectively. I-V behavior of device with configuration (a) ITO/Fc-1/Au, and (b) ITO/Fc-2/Au.

25. Thickness dependent resistive-switching behavior of ITO/Fc-2/Al

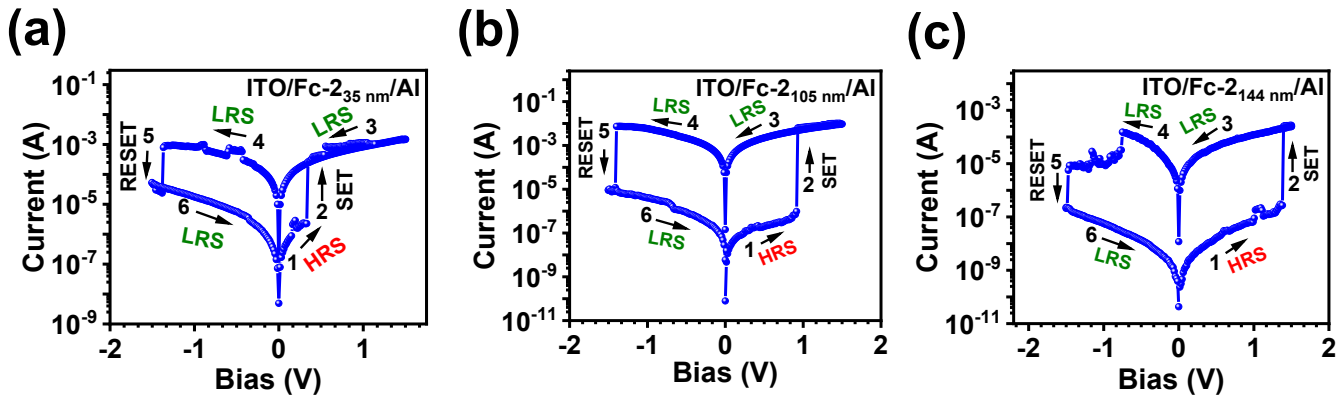

Figure S28: Thickness dependent memory characteristic of the device ITO/Fc-2/Al, at different thin film thickness of (a) 35 nm, (b) 105 nm, and (c) 144 nm.

26. Spectro-electrichemical characterization of device ITO/Fc-2/ITO

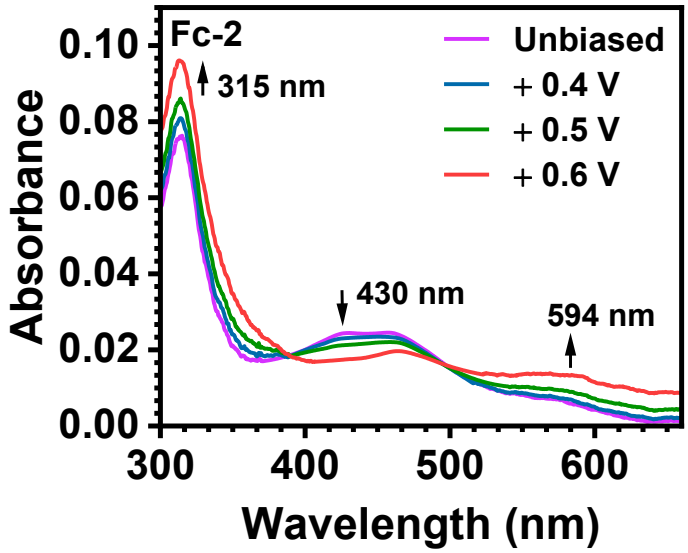

Figure S29: Spectro-electrochemical response of the ITO/Fc-2/ITO device. Upon application of positive bias voltages of + 0.4 V, + 0.5 V, and + 0.6 V, a gradual quenching of the absorption band at 430 nm is observed, with the emergence of a new absorption band at 594 nm.

27. Energy level diagram of Fc-1, and Fc-2 for isolated system

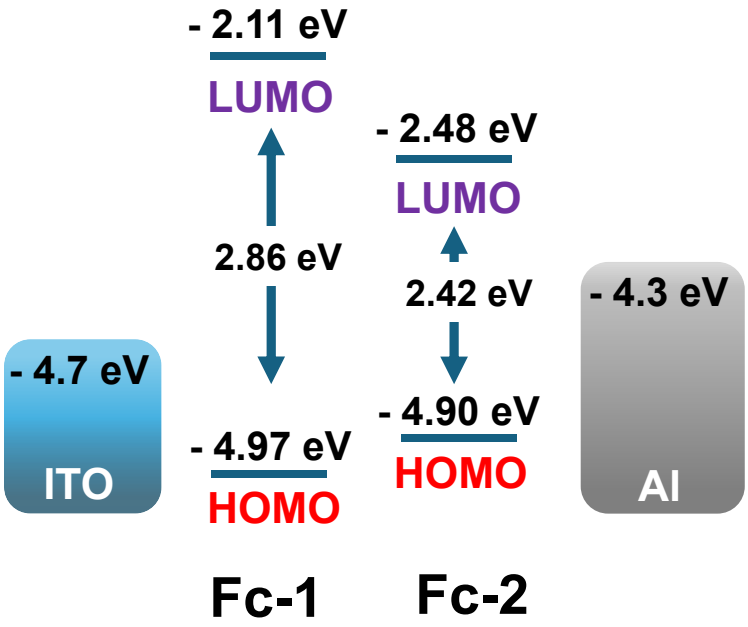

Figure S30: Energy profile showing HOMO and LUMO energy levels of Fc-1 and Fc-2 molecules.

The energy profile of Fc-1 and Fc-2, relative to the Fermi levels of the bottom ITO and top Al electrodes, reveals that the HOMO level of Fc-2 lies closer to the Fermi level of ITO than that of Fc-1. This alignment favors easier oxidation of Fc-2. Additionally, Fc-2 exhibits a narrower HOMO–LUMO bandgap, which promotes more efficient electron transfer within the device.

28. Comparison of performance for resistive-switching devices

Table S9. Comparison table for organic molecule-based resistive-switching device performance

S. No.	Device configuration	Switching threshold (V)		ON/ OFF ratio	Active layer thickness (nm)	Memory type	Memory Mechanism	Refs.
		SET	RESET					
1	ITO/Fc-2/Al	+ 0.69	1.45	10^4	80	Flash	Redox	This work
2	ITO/Fc-1/Al	+ 1.4	- 1.7	10^3	82	Flash	Redox	This work
3	Au/PI-xFC/ITO	+ 1.4	3.2	10^3	50	Flash	Charge transfer (CT)	Hao et al.[3]
4	ITO/PMMA/ Al	- 1.7	+ 4.5	--	50	Flash	Charge trapping	Singh et al.[4]
5	Au//ferrocene -6FDA/ DHTM//ITO	+ 1.5	3	10^4	50	Flash	CT	Tian et al.[5]
6	Ag/MP1/Pt	+ 2	3	10^3	28	Flash	Conductive filament	Zhang et al.[6]
7	Al/P(DTPDI-Fc)/ITO	- 2	-	10^3	120	WORM	Redox + CT	Han et al.[7]
8	ITO/FPArGO /Al	+ 2.1	- 1.9	10^2	50	Flash	Redox + Charge trapping	Jin et al.[8]
9	TO/PFcFE1/ Al	- 1	+ 2	10^3	50	Flash	Redox	Xiang et al.[9]
10	TO/PFcFE2/ Al	- 0.7	+ 3.0	10	50	Flash	Redox	Xiang et al.[9]
11	TO/PFcFE3/ Al	- 0.5	+ 3.2	10^2	50	Flash	Redox	Xiang et al.[9]
12	ITO/Ferrocene Functionalized Quinoxaline/ Al	- 1.0	-	10^4	-	WORM	Redox + CT	Gayathri et al.[10]
13	ITO/Ferrocene Functionalized Quinoxaline/ Al	- 1.3	-	10^4	-	WORM	Redox + CT	Gayathri et al.[10]

14	ITO/HBPI-Fc/Al	+ 2.5	2.7	10^4	50	Flash	Redox + Charge trapping	Tan et al.[11]
15	ITO/BDDE-HBPI-Fc/Al	+ 3.2	3.3	10^4	50	Flash	Redox + Charge trapping	Tan et al.[11]
16	ITO/Py-Fc/Al	1.6	+ 3.0	10^3	60	Flash	Redox + CT	Li et al.[12]

29. References

1 T. R. L. C. Paixão, *ChemElectroChem*, 2020, **7**, 3414–3415.

2 S. Goswami, A. J. Matula, S. P. Rath, S. Hedström, S. Saha, M. Annamalai, D. Sengupta, A. Patra, S. Ghosh, H. Jani, S. Sarkar, M. R. Motapothula, C. A. Nijhuis, J. Martin, S. Goswami, V. S. Batista and T. Venkatesan, *Nat Mater*, 2017, **16**, 1216–1224.

3 R. Hao, N. Jia, G. Tian, S. Qi, L. Shi, X. Wang and D. Wu, *Mater. Des.*, 2018, **139**, 298–303.

4 D. Singh, P. N. Gunawardene, M. S. Workentin and G. Fanchini, *Appl. Phys. Lett.*, 2024, **125**, 073505.

5 G. Tian, S. Qi, F. Chen, L. Shi, W. Hu and D. Wu, *Appl. Phys. Lett.*, 2011, **98**, 203302.

6 M. Zhang, C. Ma, D. Du, J. Xiang, S. Yao, E. Hu, S. Liu, Y. Tong, W. Y. Wong and Q. Zhao, *Adv. Electron. Mater.* 2020*,* **6***,* 2000841.

7 Y. Han, J. Shen, Q. Zhao, M. Zhou, D. Zhu, C. Hande, F. Zhou, H. Dong and Q. Zhang, Adv. Funct. Mater., 2023, **33**, 2308106

8 C. Jin, J. Lee, E. Lee, E. Hwang and H. Lee, *ChemComm*, 2012, **48**, 4235–4237.

9 J. Xiang, T. K. Wang, Q. Zhao, W. Huang, C. L. Ho and W. Y. Wong, *J. Mater. Chem. C Mater.*, 2016, **4**, 921–928.

10 R. Gayathri, M. Akshaya, P. M. Imran, N. S. P. Bhuvanesh and S. Nagarajan, *Chem. Asian J.,* 2025, **20**, 202401888.

11 H. Tan, H. Yu, Y. Song, S. Zhu, B. Zhang, H. Yao and S. Guan, *J. Polym. Sci. A Polym. Chem.*, 2018, **56**, 505–513.

12 Y. Li, X. Zhu, Y. Li, M. Zhang, C. Ma, H. Li, J. Lu and Q. Zhang, *ACS Appl. Mater. Interfaces*, 2019, **11**, 40332–40338.